doi:10.1016/j.jmb.2009.04.033 J. Mol. Biol. (2009) 392, 630–644

JMB

Available online at www.sciencedirect.com

ScienceDirect

ELSEVIER

Structural Basis for Bivalent Smac-Mimetics Recognition in the IAP Protein Family

Federica Cossu[1]†, Mario Milani[1,2]†, Eloise Mastrangelo[1,2], Patrice Vachette[3], Federica Servida[4], Daniele Lecis[5], Giulia Canevari[1], Domenico Delia[5], Carmelo Drago[6], Vincenzo Rizzo[6], Leonardo Manzoni[6,7], Pierfausto Seneci[6,8], Carlo Scolastico[6,8] and Martino Bolognesi[1]*

[1]*Department of Biomolecular Sciences and Biotechnology, University of Milano, Via Celoria 26, I-20133, Milano, Italy*

[2]*CNR-INFM S3, National Research Center on Nanostructure and BioSystems at Surfaces, Via Campi 213/A, 41100-Modena, Italy*

[3]*Institut de Biochimie et de Biophysique Moléculaire et Cellulaire, UMR8619 CNRS, Université Paris-Sud, IFR115, F-91405 Orsay, France*

[4]*Fondazione Matarelli, Department of Medical Farmacology, Chemotherapy and Toxicology, University of Milano, Via Vanvitelli 32, I-20129 Milano, Italy*

[5]*Istituto Nazionale dei Tumori, Via Venezian 1, I-20133, Milano, Italy*

[6]*Centro Interdisciplinare Studi bio-molecolari e applicazioni Industriali (CISI), University of Milano, Via Fantoli 16/15, I-20138, Milano, Italy*

[7]*CNR–ISTM, Via Fantoli 16/15, I-20138, Milano, Italy*

XIAP is an apoptotic regulator protein that binds to the effector caspases -3 and -7 through its BIR2 domain, and to initiator caspase-9 through its BIR3 domain. Molecular docking studies suggested that Smac-DIABLO may antagonize XIAP by concurrently targeting both BIR2 and BIR3 domains; on this basis bivalent Smac-mimetic compounds have been proposed and characterized. Here, we report the X-ray crystal structure of XIAP-BIR3 domain in complex with a two-headed compound (compound 3) with improved efficacy relative to its monomeric form. A small-angle X-ray scattering study of XIAP-BIR2BIR3, together with fluorescence polarization binding assays and compound 3 cytotoxicity tests on HL60 leukemia cell line are also reported. The crystal structure analysis reveals a network of interactions supporting XIAP-BIR3/compound 3 recognition; moreover, analytical gel-filtration chromatography shows that compound 3 forms a 1:1 stoichiometric complex with a XIAP protein construct containing both BIR2 and BIR3 domains. On the basis of the crystal structure and small-angle X-ray scattering, a model of the same BIR2-BIR3 construct bound to compound 3 is proposed, shedding light on the ability of compound 3 to relieve XIAP inhibitory effects on caspase-9 as well as caspases -3 and -7. A molecular modeling/docking analysis of compound 3 bound to cIAP1-BIR3 domain is presented, considering that Smac-mimetics have been shown to kill tumor cells by inducing cIAP1 and cIAP2 ubiquitination and degradation. Taken together, the results reported here provide a rationale for further development of compound 3 as a lead in the design of dimeric Smac mimetics for cancer treatment.

**Corresponding author.* E-mail address: martino.bolognesi@unimi.it.

† F.C. and M.M. contributed equally to this work.

Abbreviations used: IAP, inhibitor of apoptosis protein; BIR, baculoviral IAP repeat; XIAP, X-linked IAP; Smac-DIABLO, second mitochondria-derived activator of caspases - direct IAP binding protein with low pI; IBM, IAP binding motif; SAXS, small-angle X-ray scattering; ITC, isothermal titration calorimetry; NSD, normalized spatial discrepancy; PEG MME, polyethylene glycol monomethyl ether.

[8]*Department of Organic and Industrial Chemistry, University of Milano, Via Venezian 21, I-20133, Milano, Italy*

Received 10 February 2009; received in revised form 15 April 2009; accepted 16 April 2009
Available online
22 April 2009

Edited by I. Wilson

Keywords: inhibition of apoptosis; Smac-DIABLO; XIAP; cIAP; pro-apoptotic drugs

Introduction

The apoptotic process involves a cascade of events that inactivate critical survival pathways in multicellular organisms.[1] Inhibition of apoptosis can prevent physiological cell death, thus contributing to the development and progression of tumor malignancy.[2] Apoptosis initiation and execution phases are both dependent on a subset of caspases (cysteine-dependent aspartyl-specific proteases[3]) that are regulated by a family of inhibitor of apoptosis proteins (IAPs[4]). By direct interaction with initiator and executioner caspases, IAPs can block cell death in response to diverse stimuli. Therefore, these critical apoptosis regulators have been recognized as attractive targets for the development of innovative therapies in the treatment of cancer and neurodegenerative diseases.[5–7]

The IAP proteins contain one to three zinc-binding baculoviral IAP repeat (BIR) domains that are required for anti-apoptotic activity.[8] Most IAPs also have a C-terminal RING domain, endowed with E3 ubiquitin ligase activity.[9,10] The BIR domains host a zinc-finger motif and are generally composed of five α-helices and a three-stranded β-sheet. Some IAPs, like cIAP1 and cIAP2, contain also a caspase-associated recruitment domain (CARD) located between the BIR3 domain and the C-terminal RING domain.[11] cIAP1 and 2 are crucial regulators of receptor-mediated apoptosis,[12,13] being able to interact with tumor necrosis factor receptor (TNFR) and tumor receptor-associated factors (TRAFs) through the first two α-helices of their BIR1 domains.[14–16] Another important member of the IAP family, the X-linked IAP (XIAP), is highly expressed in many human tumor cell lines and in tumor-affected tissues from patients.[17,18] XIAP selectively targets initiator caspase-9 through its XIAP-BIR3 domain,[19] whereas it inhibits both executioner caspase-3[20] and caspase-7[21] by means of the XIAP-BIR2 domain and, particularly, the domain's N-terminal, known as the linker region (lk).

The inhibitory function of different IAPs is antagonized by the second mitochondria-derived activator of caspases - direct IAP binding protein with low pI (Smac-DIABLO[22,23]), an elongated α-helical dimeric protein of 40 kDa, released from the mitochondria. Structural and binding studies show that Smac-DIABLO binds to the XIAP-BIR3 domain through a specific IAP binding motif (IBM), built by its N-terminal tetrapeptide Ala-Val-Pro-Ile (AVPI).[24] Smac AVPI competes directly with a similar tetrapeptide (ATPF) of the activated caspase-9[21] promoting the release of the protease from the IAP complex. When IAPs are over-expressed, Smac-DIABLO may not be sufficient to overcome the inhibitory effect on caspases. In such cases, synthetic IBM-like molecules (Smac-mimetics) may be employed to relieve caspase binding, thereby promoting apoptosis in malignant cells. Along these lines of thought, and in order to avoid intrinsic limitations posed by peptide compounds, several laboratories have been actively designing Smac peptidomimetics and non-peptidomimetics with improved binding affinities, proper cell-permeability, *in vivo* stability and bioavailability,[25,26] as potential drug leads for new cancer therapeutic approaches.

Since *in silico* molecular docking studies suggested that Smac-DIABLO may bind simultaneously to XIAP-BIR2 and -BIR3 domains,[24] bivalent Smac-mimetic compounds, targeting XIAP-BIR2 and -BIR3 domains, have been proposed and characterized.[27,28] In particular, Li *et al.* synthesized a two-headed compound (Fig. 1, compound 3) with improved efficacy, relative to its monomeric form (Fig. 1, compound 2), in caspase-3 activation assays on HeLa cells extracts, and with high potency in caspase-9 activation *in vitro* (K_i = 0.12 μM).[27] Such results suggest co-inhibition of XIAP-BIR2 and -BIR3 domains by compound 3. Additionally, *in vivo* tests on a human glioblastoma cell line show that compound 3 synergizes with both TNFα and TNF-related apoptosis-inducing ligand (TRAIL) in inducing caspase activation and cell death, while Western blot analysis shows the specificity of compound 3 for cIAP1 and cIAP2.[27] Recently, it was shown that compound 3 treatment of a human tumor (HCC461), xenografted into mice, reduced the size of the

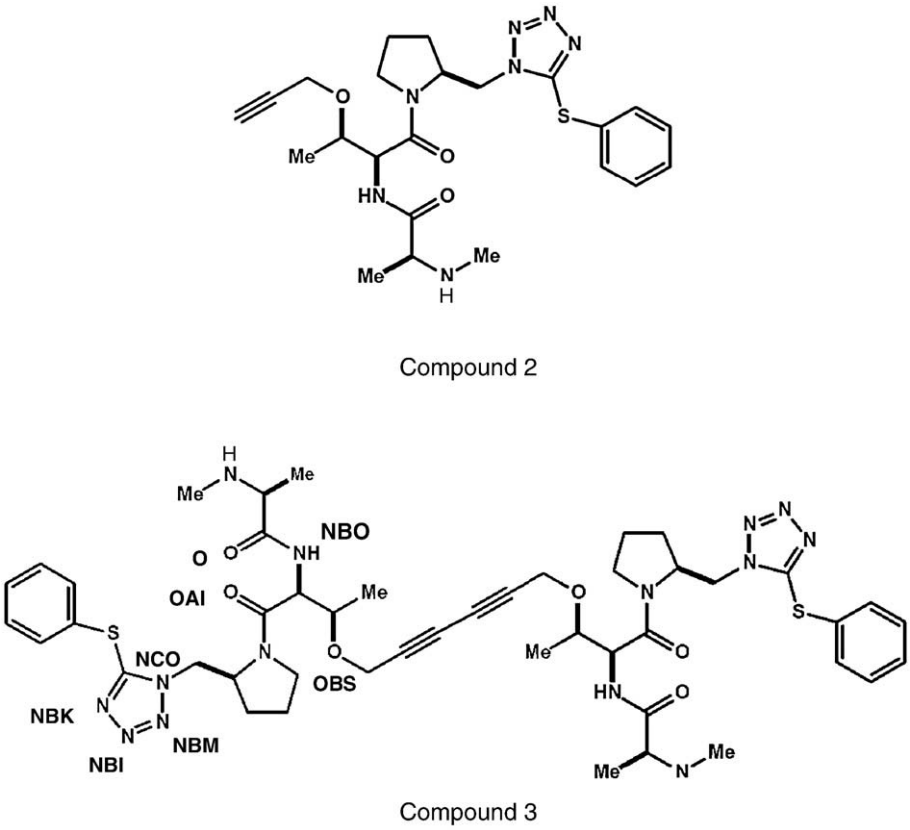

Fig. 1. Structures of the monomeric compound 2 and its bivalent form, compound 3; each interacting atom of compound 3 is named.

neoplasm and, within the treatment group, 40% of the animals remained tumor-free at the end of the experiment.[29] However, details of the interaction between the bivalent compound 3 and XIAP (or cIAP1, cIAP2) have not been described.

Here, we report the X-ray crystal structure of XIAP-BIR3 domain in complex with compound 3, at 3.0 Å resolution, together with melting temperature assays, fluorescence polarization binding assays, and cytotoxicity tests on the human HL60 leukemia cell line. The crystal structure highlights a specific network of interactions supporting XIAP-BIR3/compound 3 recognition, that are reminiscent of those described for XIAP-BIR3/AVPI[24] and XIAP-BIR3/monovalent Smac-mimetic compounds,[30–32] or for the XIAP-BIR3/bivalent Smac-mimetic peptide.[33] The capability of compound 3 to bind the BIR2 domain was assessed experimentally by microcalorimetric assays. Besides, we show that the binding mode of compound 3 to the BIR2 domain, analyzed by *in silico* docking, is comparable to those observed experimentally for the BIR3 domain. The simultaneous binding of compound 3 to BIR2 and BIR3 domains was further investigated through gel-filtration chromatography and small-angle X-ray scattering (SAXS) experiments, providing a low-resolution structure of a XIAP construct, including the N-terminal segment of the BIR2 domain (lkBIR2BIR3) in the presence/absence of the dimeric compound. Finally, we present a molecular modeling/docking analysis, and propose binding modes for compound 3 to cIAP1-BIR3 domains. The results here reported have implications for the development of high-affinity lead compounds able to bind the three IAP family members XIAP, cIAP1 and cIAP2.

Results and Discussion

Synthesis and choice of dimeric Smac mimetics

The Smac-mimetic compounds considered in this study are the bivalent compound 3 in comparison with its monomeric homolog compound 2 (Fig. 1), which were synthesized as described.[27] The bivalent compound 3 was taken into consideration in order to study the roles of the two inhibitory heads that can both interact with XIAP-BIR2 and -BIR3 domains within the same XIAP protein molecule. Earlier, compound 3 had shown enhanced efficacy on caspase-3 activation in HeLa cells extracts, relative to its monomeric counterpart.[27] Moreover, besides XIAP, compound 3 exhibits promising ability to bind to cIAP1 and cIAP2,[27] thus potentially preventing the compensative expression of other IAP family members that would impair its pro-apoptotic action.

Smac-mimetics binding assays

Monomeric compound 2 and dimeric compound 3 were tested for their *in vitro* binding to XIAP-BIR3 and -lkBIR2BIR3, using two reported assay formats.[34,35] The K_i values (Table 1) show that compound 3 is a better inhibitor for both XIAP-BIR3 and -lkBIR2BIR3 relative to compound 2. The higher affinity of compound 3 (IC_{50} of 230.8±32.8 nM) for XIAP-BIR3, compared to that displayed by compound 2 (IC_{50} of 387.0±33.5 nM), can be explained by the dimeric nature of compound 3. In fact, for a well known statistical effect,[36] the macroscopic dissociation constant of a divalent ligand can be lower by a factor of 2–4 relative to that measurable for the corresponding monomeric ligand with identical microscopic dissociation constant (free energy of interaction). This is true under the assumption of truly independent sites, which is an ideal situation. The observed ratio (1/1.7) is in keeping with such an explanation, and suggests a modest destabilizing interaction between the two sites upon binding.

The monomeric compound 2 shows an IC_{50} value for XIAP-lkBIR2BIR3 similar to that displayed for XIAP-BIR3 (Table 1). Such behavior is expected, since BIR3 is the high-affinity binding site for the Smac N-terminal AVPI peptide ($K_d \sim 500$ nM), while BIR2 is the low-affinity binding site ($K_d \sim 10$ μM) for the same peptide.[35] Thus, the presence of the BIR2 domain in the XIAP-lkBIR2BIR3 construct should not affect the measured IC_{50} for a monomeric compound. In contrast, simultaneous binding of compound 3 to XIAP-BIR2 and -BIR3, as shown by gel-filtration analysis and the SAXS structure (see below), results in a significant increase in potency (IC_{50} of 3.3±0.6 nM; Table 1, right).

Microcalorimetric assays

Isothermal titration calorimetry (ITC) can provide accurate information on the thermodynamic contributions of enthalpy and entropy changes to free energies of binding, directly measuring the heat exchanged during a biomolecular binding event, providing an estimate of the dissociation constant. ITC experiments run on the protein domains here revealed a micromolar affinity of the XIAP-BIR2 domain for both compound 2 (K_d=9.0±1.6 μM; Supplementary Data Fig. S4A) and compound 3 (K_d=3.0±0.6 μM; Supplementary Data Fig. S4B). These results complement the information provided by analytical gel-filtration and SAXS experiments, demonstrating the actual binding of BIR2 to compound 3, proving that the enhanced affinity of compound 3 for lkBIR2BIR3 is due to simultaneous binding of the divalent molecule to two distinct protein domains.

Table 1. Cytotoxicity and *in vitro* IC_{50} values of compounds 2 and 3

	Cytotoxicity	Fluorescence binding assays	
	IC50 (μM)	IC50 (nM)	
Compound	HL60	XIAP-BIR3	XIAP-lkBIR2BIR3
2	7.00±1.64	387.0±33.5	295.4±61.5
3	0.07±0.02	230.8±32.8	3.3±0.6

Cytotoxic activity *in vivo* displayed by compounds 2 and 3 on the HL60 leukemia cancer cell line, determined in three independent experiments. *In vitro* IC_{50} values of compounds 2 and 3 on XIAP-BIR3 and XIAP -lkBIR2BIR3 determined by fluorescence binding assays in three independent experiments. All data are expressed as mean±SD.

Cell based inhibition assays

Compounds 2 and 3 were tested for 72 h on HL60 leukemia cells. The results given in Table 1 indicate that the IC_{50} of the dimeric compound 3 (0.07 μM) is 100-fold lower than that of the monomeric compound 2 (7 μM), underlining its "drug-like" potential. Moreover, it has been reported recently that various human cancer cell lines undergo apoptosis upon treatment with compound 3, without requiring exogenous pro-apoptotic stimuli or co-treatment with chemotherapeutic agents.[29]

Crystal structures of XIAP-BIR3/compound 3 complex

Analysis of compound 3 binding mode to the XIAP-BIR3 domain was addressed through X-ray crystallography. XIAP-BIR3/compound 3 3D structure was solved by the molecular replacement method at 3.0 Å resolution (R_{gen}=23.1%, R_{free}=31.1%, eight BIR3 molecules per asymmetric unit; see Materials and Methods). As reported earlier,[20,21,24] the XIAP-BIR3 domain is composed of five α-helices and a three-stranded β-sheet, hosting a zinc-finger motif (Fig. 2a). Inspection of difference Fourier maps at various stages of the crystallographic refinement revealed strong residual electron density located in the IBM groove (the XIAP-BIR3/AVPI recognition groove), comprised between the β3 strand and the α3 helix (Fig. 2a and b), for all the eight molecules in the crystal asymmetric unit. One head of compound 3 could be modeled promptly in such residual densities, and accordingly refined. Therefore, the refined model is composed of eight BIR3 molecules (XIAP residues 253±2 through 351±5) and eight compound 3 molecules, each of which has an inhibitory head bound to BIR3 and the other devoid of any contact to the protein. The eight asymmetric unit copies of the XIAP-BIR3/compound 3 complex can be divided into two structural groups: group I, subunits A, C, E, and G; and group II, subunits B, D, F, and H. For the four molecules in group I it was possible to model the C-terminal α-helix only up to residue 347±1; in group I, the free head of compound 3 is fully disordered in the solvent. On the other hand, for the molecules belonging to group II, the entire C-terminal α-helix (up to residue 357±1) could be modeled, and compound 3 is entirely defined (two heads) in the electron density. However, in group II, pairs of compound 3-free heads (B and D; F and H) share common locations in the asymmetric unit. The

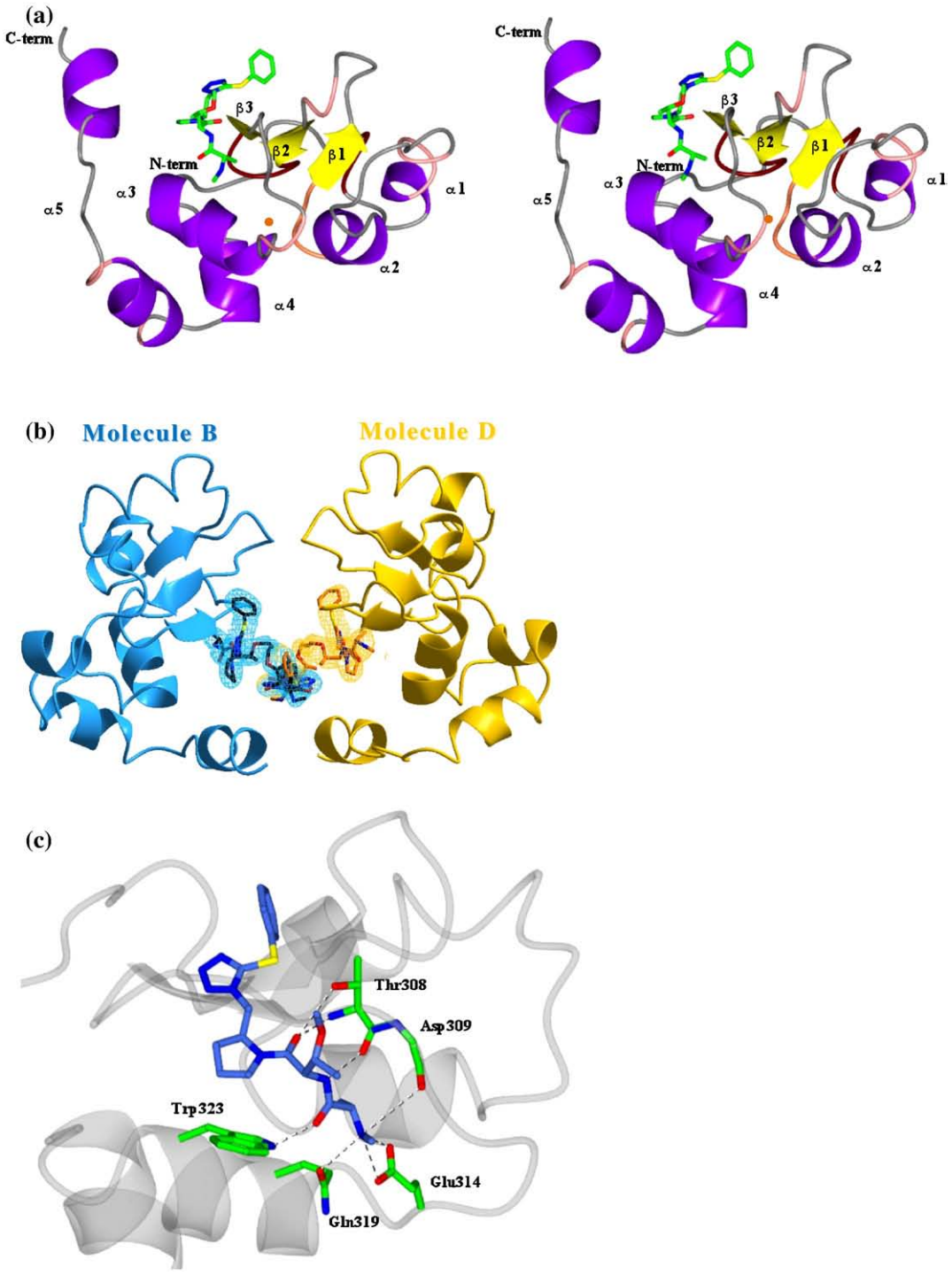

Fig. 2. (a) A 3D stereo-view of the overall architecture of XIAP BIR3 domain. The five α-helices building BIR3 are shown in purple, the three anti-parallel β-strands are shown in yellow; note the extended C-terminal α5 helix. The core zinc atom is represented as a coral sphere. The difference electron density falls in the IBM groove between the β3 strand and the α3 helix, where one monovalent part of compound 3 binds. (b) Detail of the crystal packing of two BIR3 molecules (B and D) in presence of compound 3: it is clear how the two free heads of compound 3 share the same electron density in correspondence to a 2-fold axis. (c) A view of the BIR3/compound 3 interaction network. The main residues involved in stabilizing interactions with compound 3 are shown in green; nitrogen atoms are shown in blue, and oxygen atoms are shown in red. The compound 3 molecule is in light blue; the main hydrogen bonds linking BIR3 and the compound 3 are shown as broken lines (drawn with CCP4 mg[58]).

matching of the location shared by two heads is clearly deduced by the shape of their electron density (Fig. 2b). We therefore modeled the superimposing heads of two ligand pairs with 0.5 occupancy, thus implying that when one half of compound 3 (e.g. free head B) occupies the observed position, half of the

Table 2. X-ray data-collection and refinement statistics for the BIR3/compound 3 complex

A. *Data collection*	
Space group	$P3_1$
Unit-cell parameters	
a = b (Å)	119.1
c (Å)	105.6
α = β (°)	90
γ (°)	120
Solvent content (%, v/v)	65.9
Molecules/per asymmetric unita.u.	8
Resolution (Å)	40.0–3.0
Mosaicity (°)	0.9
№ of unique reflections	33,440 (4861)
Completeness (%)	99.8 (99.9)
Redundancy	3.6 (3.7)
R_{merge}[a] (%)	10.1 (64.0)
Average I/σ (I)	13.3 (2.2)
B. *Refinement*	
R-factor[b] (%)	23.1
R_{free}[c] (%)	31.1
r.m.s.d. from ideal	
Bond lengths (Å)	0.011
Bond angles (°)	2.042
Average protein B-factor (Å^2)	73.1
Average compound 3 B-factor (Å^2)	50.6
Ramachandran plot	
Residues in most favored regions (%)	80.7
Residues in additionally allowed regions (%)	19.0
Residues in generously allowed regions (%)	0.3

Values in parentheses are for the highest resolution shell.
[a] $R_{merge} = \Sigma\ |I - (I)|\ /\ \Sigma\ I \times 100$, where I is the intensity of a reflection and (I) is its average intensity.
[b] $R\text{-factor} = \Sigma\ |F_o - F_c|\ /\ \Sigma\ |F_o| \times 100\%$
[c] R_{free} for cross-validation was calculated with 5% of reflections that were selected at random and were not included in the refinement.

other compound 3 (e.g. free head D) is disordered in the solvent and *vice versa*. Such peculiar feature can be explained by the mutual orientation of the B-D and F-H protein dimers in group II. In fact, in each dimer a couple of antiparallel C-terminal α-helices closes the ligand in a sort of "hug", restraining the conformational freedom of the free head that results in the observed superposition (Fig. 2b).

Superposition of the eight BIR3 protein domains (amino acids 253–344) yields r.m.s.d. values of 0.13–0.24 Å among molecules belonging to the same structural group, and 0.46–0.52 Å when comparing the two different structural groups. Data collection and refinement statistics are given in Table 2, together with stereochemical quality of the structure.

Structure and recognition in the XIAP-BIR3/compound 3 complex

Superposition of the eight independent molecules in the crystal asymmetric unit shows contained conformational variability for the protein residues interacting with compound 3. In particular, all the atoms from amino acids falling within 4.0 Å from the ligand (292, 297–299, 306–310, 314, 319, and 323–324) have an r.m.s.d. of 0.4±0.1 Å. Comparison of the crystal structures shows that the protein/ligand interactions stabilizing the XIAP-BIR3/compound 3 complex resemble those observed in the XIAP-BIR3/Smac-DIABLO structure (PDB code 1G73;[24]; r.m.s.d. 0.38 Å) and in the XIAP-BIR3/ bivalent Smac-mimetic peptide (the cyclized $(CH_3\text{-AKPF})_2$ peptide; PDB code 2VSL[33]). One of the two heads of compound 3 is bound to the IBM groove (roughly lined by residues Lys297, Thr308-Asp309, Glu314, and Trp323), exchanging hydrogen bonds and van der Waals contacts with residues Gly306, Thr308, and Asp309, located in the β3 strand, with Glu314 and Gln319 belonging to the β3 – α3 loop, and with Trp323 and Tyr324 in the α3 helix (Table 3, left and Fig. 2c). In particular, the N-terminal part of the compound 3 head is bound to the protein mainly by electrostatic interactions, while mimicking an antiparallel β-sheet, as shown for the Ala1-Val2 N-terminal residues of Smac-DIABLO and for the Ala1-Lys2 N-terminal residues of the bivalent Smac-mimetic peptide.[33] In contrast, the remaining part of the same head (pyrrolidine, tetrazole and phenyl rings) provides van der Waals interactions only. In detail, the N-terminal-bound end of compound 3 exchanges a salt bridge with Glu314 (2.8±0.2 Å; distance averaged over the eight independent molecules) and a loose hydrogen bond with

Table 3

XIAP-BIR3/compound 3 (crystal structure)			XIAP-BIR2/compound 3 (docking model)			cIAP1-BIR3/compound 3 (docking model)		
Residue	Interaction	Mean (Å)	Residue	Interaction	Dist. (Å)	Residue	Interaction	Dist. (Å)
Thr 308	N-OAI	3.0	Lys 208	N-OAI	2.7	Arg 308	N-OAI	3.1
	N-O	3.1		O-NBO	2.7		O-NBO	2.9
	$O^{\gamma 1}$-OBS	3.4					O-OBS	3.0
Glu 314	$O^{\varepsilon 1}$-N	2.8	Asp 214	$O^{\delta 2}$-N	2.8	Asp 314	$O^{\delta 2}$-N	2.7
	$O^{\varepsilon 2}$-N	2.8						
Gln 319	$O^{\varepsilon 1}$-N	3.4	Glu 219	$O^{\varepsilon 1}$-N	2.8	Glu 319	$O^{\varepsilon 1}$-N	2.5
				$O^{\varepsilon 1}$-O	3.6			
Trp 323	$N^{\varepsilon 1}$-O	3.1	His 223	$N^{\varepsilon 1}$-O	3.8	Trp323	$N^{\varepsilon 1}$-O	3.2
				Nε2-O	3.0			

Left: Average distances (in Å) between atoms of compound 3 and BIR3 amino acids involved in the main protein/ligand interactions, as observed in the crystal structure. Centre: Compound 3/XIAP-BIR2 interactions from the docking model. Right: Compound 3/cIAP1-BIR3 interactions from the docking model.

Gln319 (3.4±0.4 Å) as observed for XIAP-BIR3/monovalent Smac-mimetic compounds (Smac005,[30] Smac010,[30] Smac037,[31] and compound 21[32]). In fact, all the bicyclic Smac-mimetic compounds terminal amines lose hydrogen bonds/van der Waals contacts with Gln319, gaining other interactions mainly involving Thr308 (Smac005 and compound 21) and Asp309 (Smac010, Smac037 and compound 21). The compound 3 methyl group (CB) is well inserted in a hydrophobic surface depression lined by Leu307 and Trp310. The next peptide plane is stabilized by hydrogen bonds with the side chain of Trp323 (3.1±0.2 Å) and the main-chain carbonyl group of Thr308 (3.1±0.3 Å). The carbonyl OAI is hydrogen bonded to the peptide N atom of Thr308 (3.0±0.2 Å) and, partially, with its side chain (3.4±0.4 Å). The following two rings (pyrrolidine and tetrazole) are involved in hydrophobic contacts mainly with Gly306, Trp323 (stacking interaction with pyrrolidine ring), and Tyr324. Finally, the terminal phenyl group is well located in a hydrophobic dip encircled by the side chains of Leu292, Lys297, and Lys299. When compared to the XIAP-BIR3/AVPI and XIAP-BIR3/bivalent Smac-mimetic peptide complexes,[33] the XIAP-BIR3/compound 3 structure shows the conservation of all electrostatic interactions, but the loss of a hydrogen bond to the main-chain carbonyl group of Gly306.

Conversely, the second head of compound 3 (when traceable in density) is not found in contact with any part of the protein in the crystal structure.

Melting temperature thermal shift assays

Thermal shift assay is an experimental technique monitoring fluorescence variations reported by a protein-bound dye during protein thermal denaturation. The method was developed originally for drug discovery, to allow rapid identification of protein ligands by screening compound libraries.[37] Since small molecules (e.g. an enzyme inhibitor) bound to a protein can affect (often stabilize) its structure, the assay monitors the variation in melting temperature (T_m) induced by ligand binding. Sypro orange, the fluorescent dye used here, binds efficiently to the unfolded protein displaying an increase of fluorescence intensity during temperature-dependent protein unfolding.[36]

The T_m values for the protein constructs considered here were shifted toward higher temperatures by the binding of both the monomeric/dimeric Smac-mimetic compounds. Taking the T_m values as indicative of increasing stabilization of the protein/ligand adducts produced, compound 2 was found to stabilize all constructs, with ΔT_m values of +10.1 degC, +9.0 degC and +14.3 degC in XIAP-BIR2, -BIR3 and -lkBIR2BIR3, respectively, while the ΔT_m values for compound 3 were +10.3 degC, +10.0 degC and +17.6 degC in XIAP-BIR2, -BIR3 and -lkBIR2BIR3, respectively. Interestingly, the stabilization of XIAP-lkBIR2BIR3 by compound 2 is lower by more than 3 degC (ΔT_m +14.3 degC) than that measured for compound 3 (ΔT_m +17.6 degC). Such findings indicate that the stabilization effects of both the monomeric and dimeric Smac mimetics on a single protein domain are similar, but that compound 3 induces higher stability for the XIAP-lkBIR2BIR3 construct. Such an effect may be explained by the simultaneous binding of compound 3 to the XIAP-BIR2 and -BIR3 domains, resulting in (i) the stabilization of the two domains, and (ii) a more compact shape of the overall protein structure. The latter structural effect is supported by the gel-filtration assays and the SAXS analysis described below. Although the effects on T_m are clear-cut, and may show a trend, such assays must be taken only as a qualitative ranking of Smac-mimetics affinity for the three BIR constructs. The main result suggested by the thermal shift assays is that all compounds bind effectively to XIAP-BIR3, and to the XIAP-BIR2 domain. (Experimental sigmoid T_m plots, as well as other experimental data given below are reported in graphical form as Supplementary Data).

Analytical gel-filtration assays

In order to check whether the crystallization conditions might have prevented the simultaneous interaction of compound 3 with two XIAP-BIR3 domains, we performed analytical gel-filtration assays using a fixed concentration of protein (33 μM) and an excess of compound 2 or 3 (5 mM). The chromatograms obtained for XIAP-BIR3 in the presence of compound 3 show a peak at an elution volume (V_e) of 10.6 ml, corresponding to the dimeric form of the protein. In the presence of compound 2, or in the absence of the Smac-mimetics, a peak at V_e of 11.8 ml, corresponding to the monomeric form is present in the chromatogram. The absence of a dimeric assembly from our crystal structure obtained in the presence of compound 3 is likely due to the crystal growth conditions, i.e. higher concentrations of protein and salt relative to the analytical gel-filtration tests.

We investigated the interaction of compound 3 with the XIAP-lkBIR2BIR3 construct. The chromatogram shows a peak shift of V_e from 10.5 ml to 10.8 ml in the presence of an excess of compound 3 (5 mM), suggesting an actual reduction of the protein volume. A more compact protein moiety is compatible with the simultaneous binding of compound 3 to the two domains of the construct, as confirmed by the SAXS data (see below). Similar results have been reported recently for two different bivalent Smac-mimetics: the bivalent cyclic peptide in Ref. 33, and the bivalent SM-164 in Ref. 28. In both cases, the presence of a divalent compound causes a shift of the GF peak toward higher V_e values, suggesting the simultaneous binding of the bivalent compounds to the BIR2 and the BIR3 domains. Moreover, in both cases, a mutation of the BIR2 domain in the IBM groove (E219R) alters the binding of the divalent compounds, indicating that the BIR2 IBM groove is directly involved in the interaction. In contrast, analytical gel-filtration in the presence of compound 2 (5 mM) shows that XIAP-lkBIR2BIR3 does not change its shape (V_e 10.5 ml).

Virtual docking of compound 3 to XIAP-BIR2

XIAP is well known to inhibit caspase-3 and -7 by means of a protein region located N-terminal to the BIR2 domain (the so-called linker region).[20,21] However, a recent study showed that additional interactions between BIR2 and caspases -3 and -7 involve a region of the BIR2 domain structurally related to the IBM groove described for the XIAP-BIR3/caspase-9 interaction.[19] The BIR2 domain IBM groove may thus strengthen the binding between XIAP and caspases -3 and -7. As a consequence, Smac-mimetics able to bind the XIAP-BIR2 IBM groove might promote caspase-3 and -7 activity in apoptosis. Moreover, compounds showing high affinity for other XIAP homologs, such as cIAPs, would enhance the apoptosis-promoting effect.

An *in silico* docking approach based on the program AutoDock4[38] was used to propose a model for compound 3 binding to XIAP-BIR2. In particular, we performed virtual docking searches using the high-resolution crystal structure of XIAP-BIR2 (PDB code 1I3O, subunit E[20]). The BIR2/Smac-mimetic complex model obtained was subsequently compared to the crystal structure of XIAP-BIR3/compound 3, considering that XIAP-BIR2 and -BIR3 domains display an amino acid sequence identity of 41.5%, and their crystal structures have an r.m.s.d. of 0.89 Å (77 C^{α} pairs). The model produced *in silico* indicated that compound 3 roughly binds to the BIR2 domain as observed experimentally for the XIAP-BIR3 domain. Moreover, the estimated binding free energy of compound 3 to BIR2 appears to be close to that obtained for the XIAP-BIR3 complex model (about −8.6 kcal/mol for XIAP-BIR2/compound 3, and −8.1 kcal/mol for -BIR3/compound 3).

Analysis of the ligand/protein interaction network in the XIAP-BIR2/compound 3 model (Fig. 3) indicates that some conservatively substituted amino acids, such as XIAP-BIR2 Lys208, Asn209, Asp214, Glu219, and His223, are predicted to be involved in productive hydrogen bonding interactions with the Smac-mimetic compound (Table 3, centre).

XIAP-lkBIR2BIR3 SAXS study

The two scattering patterns of XIAP-lkBIR2BIR3 solutions in the absence/presence of the compound 3 inhibitor, are shown in Fig. 4a. They are composite curves obtained by combining data recorded at low (small-angle) and higher (wider-angle) concentrations, as explained in Materials and Methods. They exhibit significant differences, suggesting that compound 3 binding causes a global conformational change in the protein. Guinier plot analysis of the two curves shows a reduction of the radius of gyration in the presence of the inhibitor, from 27.7±0.3 Å to 24.6±0.3 Å. $I(0)/c$ values yield a molecular mass estimate of about 28 kDa and 29 kDa for the apo protein and the complex with the inhibitor, respectively, in good agreement with the values of 28,847 Da derived from the protein amino acid sequence, and of 971 Da for the inhibitor. This agreement shows that protein samples at a concentration of 1 mg/ml were essentially free of intermolecular interactions. The distance (or pair) distribution functions $p(r)$ (Fig. 4b) yield values of 105±5 Å and 29.1±0.2 Å for the maximal diameter and radius of gyration of the apo protein, respectively, to be compared with 95±5 Å and 25.2±0.2 Å, respectively, obtained in the presence of the inhibitor. All these results point to a conformational transition of XIAP-lkBIR2BIR3 from an extended to a more compact conformation upon inhibitor binding. The $p(r)$ profile of the apo protein is broadly spread, with a first peak around 20 Å and a clear shoulder between 35 and 60 Å, corresponding predominantly

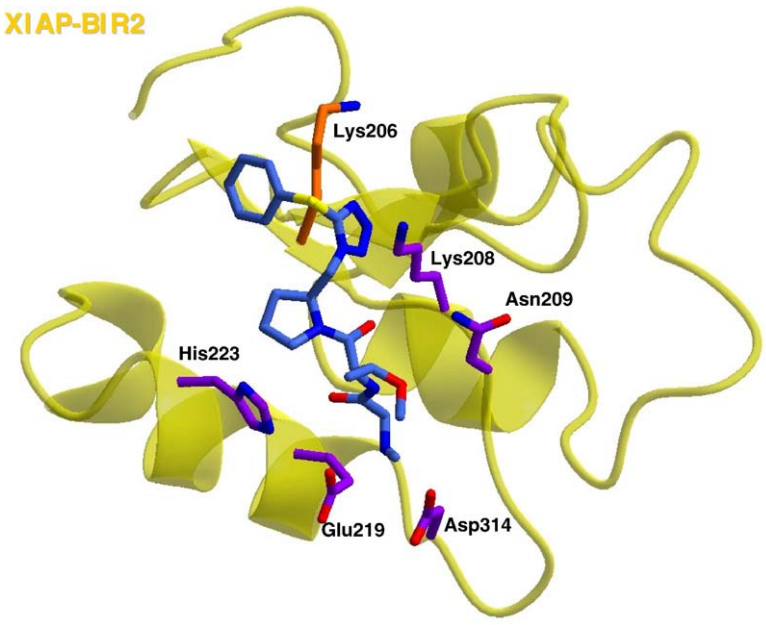

Fig. 3. Virtual docking models for the XIAP-BIR2/compound 3 complex. The main residues involved in stabilizing interactions with BIR2/compound 3 (labeled) are shown in purple. The compound 3 molecule is shown in light blue; and the protein non-interacting residue is shown in orange. Nitrogen atoms are shown in blue, and oxygen atoms are shown in red (drawn with CCP4 mg[58]).

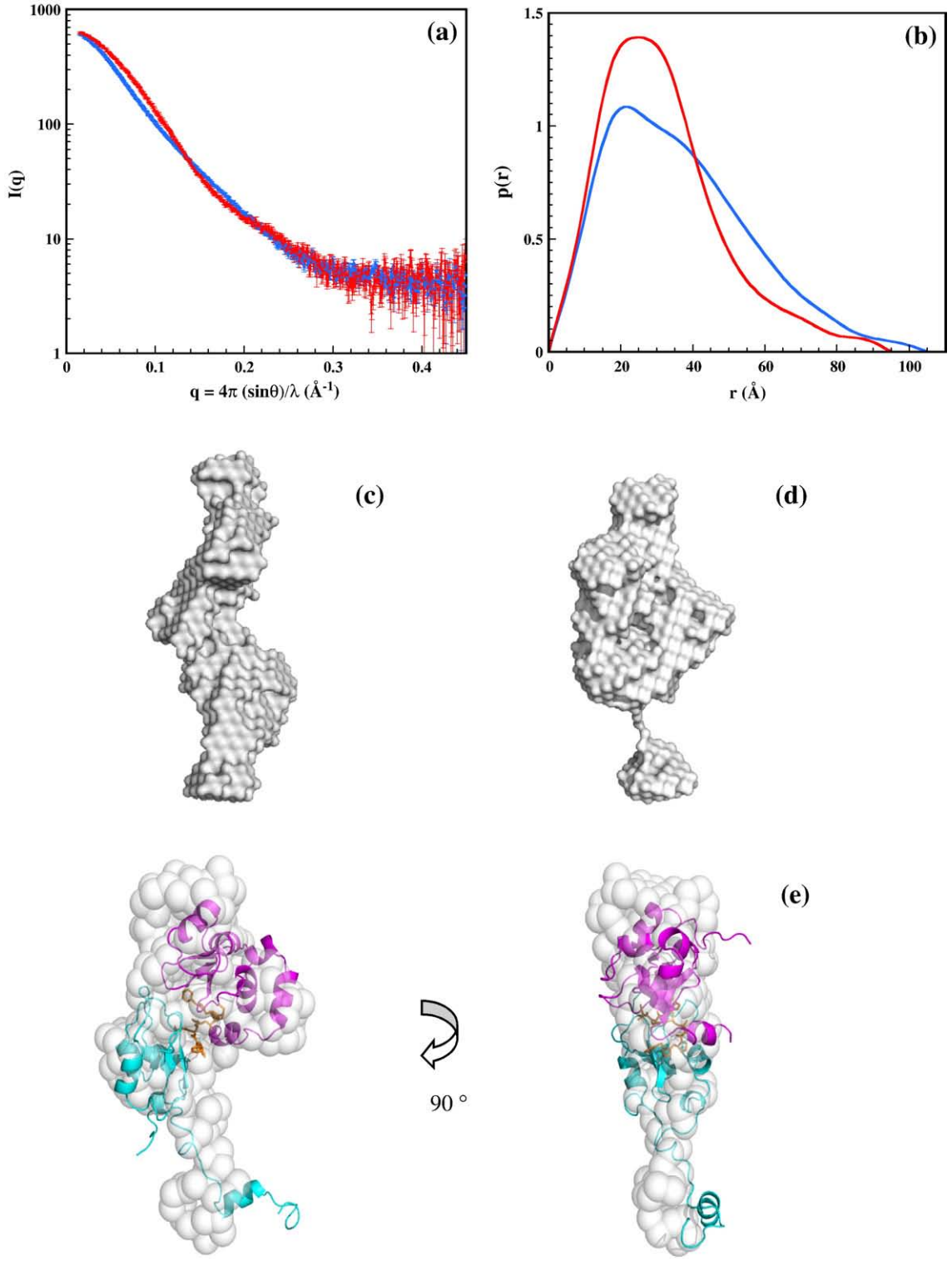

Fig. 4. XIAP-lkBIR2BIR3 SAXS patterns. The scattering patterns (a) and distance (or pair) distribution functions $p(r)$ (b) of XIAP-lkBIR2BIR3 solutions in the absence/presence of compound 3 are shown in blue and red, respectively. c and d, Most typical SAXS models of XIAP-lkBIR2BIR3 in the absence (c) or in the presence (d) of compound 3 obtained with the program Dammin (surfaces are shown in white). (e) XIAP-lkBIR2BIR3/compound 3 model (BIR2 in cyan, BIR3 in magenta, and compound 3 in orange) superimposed on the most typical dummy residue model obtained with Gasbor (dummy atoms are shown as white spheres). The left-hand and right-hand views are related by a 90° rotation around a vertical axis. The figure was realized using Pymol [http://pymol.sourceforge.net/].

to intra- and interdomain distances, respectively, while most distances are found in a narrow range (15–45 Å) in the presence of the inhibitor. This suggests that the BIR2 and BIR3 structured domains are well resolved in the apo protein and likely mobile around a flexible linker. Conversely the

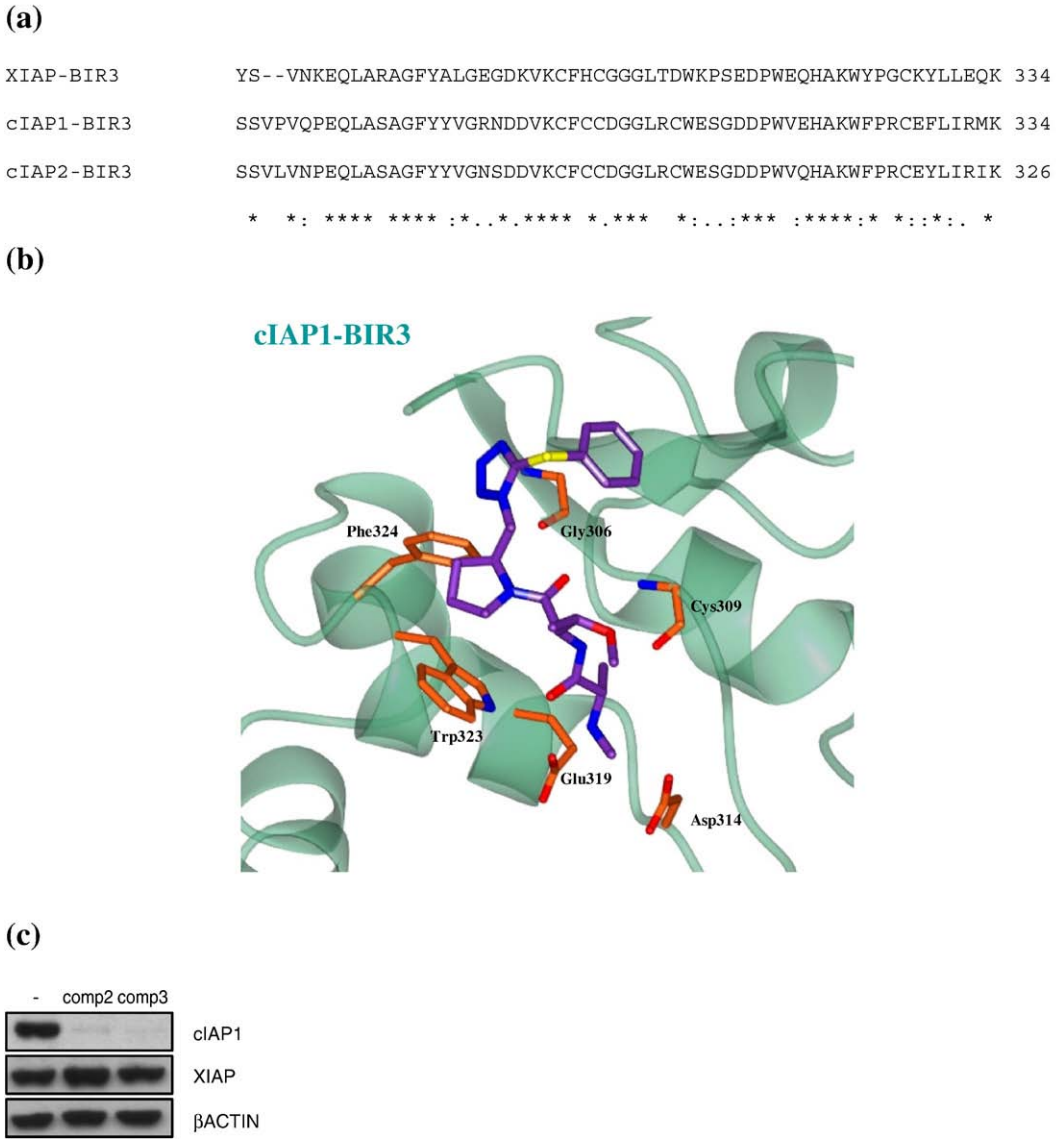

Fig. 5. (a) Alignment between XIAP-BIR3, cIAP1-BIR3 and cIAP2-BIR3 domains: "**.**" and "**:**" stand for half-conservative and conservative substitutions, respectively. "*****" stands for conserved residues. (b) Model of the interaction of compound 3 with cIAP1-BIR3. Compound 3 is shown in purple and interacting residues are represented in orange. (c) cIAP1 degradation experiment in the presence of compounds 2 and 3. Proteins were revealed by Western blot using antibodies specific for XIAP, cIAP1 and βActin. The symbol "-" is for the negative control of the cells in the absence of the Smac-mimetics.

bivalent inhibitor binds to both active sites (one on each domain), bringing BIR2 and BIR3 in closer proximity, thereby leading to the narrower distance distribution observed.

The shape of XIAP-lkBIR2BIR3 in the absence/presence of compound 3 was investigated *ab initio* using programs Dammin[39] and Gasbor.[40] Ten low-resolution models were calculated for each conformation before superimposition, to determine the most typical model. All calculated scattering patterns are in excellent agreement with the experimental data. Values of ~1.2 and ~1.0 of the normalized spatial discrepancy (NSD) are obtained for the protein in the absence/presence of compound 3, respectively, showing that all shapes in a series are very similar. The shape of XIAP-lkBIR2BIR3 in the absence of the bivalent Smac-mimetic appears to be elongated and rather thin, large enough to accommodate the two domains in non-contiguous positions together with the linker (Fig. 4c). This also explains the higher NSD value commonly observed with elongated particles, since it is sensitive to minor local differences between globally very similar shapes. In contrast, XIAP-lkBIR2BIR3 in the presence of compound 3 shows a broader compact shape, large enough to accommodate the two domains together with a small appendage that may be representative of the N-terminal linker (Fig. 4d).

It was possible to model the interaction between BIR2 and BIR3 domains in the presence of the ligand using the peculiar crystallographic arrangements of dimers observed in our structure as described in

Materials and Methods. Figure 4e shows the model for XIAP-lkBIR2BIR3 complexed with compound 3 thus obtained, superimposed on the most typical SAXS dummy residue model for XIAP-lkBIR2BIR3/compound 3. The dummy residue model fits quite satisfactorily our XIAP-lkBIR2BIR3 model that was assembled on the basis of independent principles. It should be noted that here we do not propose a high-resolution model of XIAP-lkBIR2BIR3 compound 3 interaction (a high-resolution model of the interaction with a different dimeric compound has been reported recently[33]) but just a low-resolution molecular shape that is in agreement with the SAXS experimental results.

Compounds 2 and 3 in cIAP degradation

It has been reported recently that Smac-mimetics may kill cancer cells *via* a mechanism involving ubiquitination and degradation of cIAP1 and cIAP2, resulting in TNFα-mediated cell death.[16,29,41] Since compound 3 was shown to interact with cIAP1 and cIAP2,[13,27] we performed a virtual docking search analyzing the possible binding mode(s) of compound 3 on the cIAP1-BIR3 domain, whose crystal structure was published recently (PDB code 3D9U, subunit A[42]).

A superposition of XIAP-BIR3/compound 3 crystal structure on the cIAP1-BIR3 domain (40 C^{α} pairs) indicates a r.m.s.d. of 0.58 Å. The two homolog BIR3 domains (XIAP-BIR3 and cIAP1-BIR3) show a sequence homology of 37% and a good conservation of the residues belonging to their IBM pockets (Fig. 5a, the cIAP1-BIR3 residues number are that of the PDB 3D9U). Among all amino acids involved in the interaction network between XIAP-BIR3 and compound 3 observed in the crystal structure, most are conserved (Gly306 and Trp323) or substituted conservatively (Asp311, Glu319, and Phe324). Only Arg308 and Cys309 are not conserved within the pocket (Fig. 5a). Nevertheless, the analysis of the predicted binding mode for compound 3 (Fig. 5b) suggests that the non-conservative substitutions should not affect its affinity for cIAP1-BIR3 (the binding free energy value for cIAP1-BIR3/compound 3 complex is −10.5 kcal/mol). The cIAP1-BIR3/compound 3 complex model suggests conservation of crucial interactions that involve the Gly306 and Arg308 backbones, the Asp314, Glu319 and Phe324 (Table 3, right and Fig. 5b). Compound 3 pyrrolidine ring establishes hydrophobic contacts to Trp323 and Phe324. Moreover, since amino acids involved in the cIAP1-BIR3/compound 3 interactions are well conserved in the cIAP2-BIR3 domain (Fig. 5a), the same interaction network might stabilize compound 3 binding to cIAP2.

The experimental approaches here adopted to characterize compound 3 binding to XIAP-lkBIR2-BIR3 led us to extend our views to cIAP1 and -2 members of the family through the simulative approaches described. Since the interactions of the Smac-mimetics with cIAP1-BIR3 predicted by the docking algorithms suggested efficient binding, as an independent approach, we carried out cIAP1 degradation experiments in the presence of both compounds 2 and 3 (similar results are shown in Ref. 43), using the MDA-MB231 cell line. In keeping with the hypothesis suggested by our docking results, Western blot analysis revealed that both the Smac-mimetic compounds were able to induce degradation of the cIAP1 protein (Fig. 5c).

As a whole, our results provide comprehensive new structural and recognition information on the interaction of Smac-mimetics with the IBM grooves of XIAP (BIR2 and BIR3 domains), of cIAP1 and cIAP2. New working grounds for the development of high-affinity lead compounds specifically binding the three members of the IAP family are thus available.

Materials and Method

Chemistry

Compounds 2 and 3 were synthesized as described.[27]

Cloning, expression and purification of human XIAP BIR domains

The cDNA coding for human XIAP was retro-transcribed from a pool of human mRNAs. The sequences coding for regions 241–356 (XIAP-BIR3), 124–356 (XIAP-lkBIR2BIR3) and 140–240 (XIAP-BIR2) were cloned in pET28(b) (Novagen), in NheI-BamHI sites. All the plasmids were used to transform *Escherichia coli* strain BL21(DE3) as described.[31] The proteins were stored in 20 mM Tris pH 7.5, 200 mM NaCl, 10 mM DTT.

Fluorescence polarization assays

Fluorescence polarization experiments were performed as described.[34,35] Briefly, the experiments were performed in black, flat-bottom 96-well microplates (GREINER BIO-ONE), and fluorescence polarization was measured with an Ultra plate reader (Tecan). For the XIAP-BIR3 construct, a fluorescently labeled Smac peptide (AbuRPF-K(5-Fam)-NH_2) (FITC-Smac[35]) was used at a final concentration of 5 nM, added to an assay buffer together with increasing concentrations of XIAP-BIR3 (0 – 20 μM). For the XIAP-lkBIR2BIR3 construct, a fluorescently labeled dimeric Smac peptide (Smac-1F[34]) was used at a final concentration of 1 nM, added to the assay buffer together with increasing concentrations of lkBIR2BIR3 (0 – 2 μM). The final volume in each well was 125 μl, with the assay buffer consisting of 100 mM potassium phosphate pH 7.5, 100 μg/ml bovine γ-globulin, 0.02% (w/v) sodium azide. After shaking for 15 min, the plate was incubated for 3 h at room temperature. Fluorescence polarization was measured at excitation and emission wavelengths of 485 nm and 530 nm, respectively. The equilibrium binding graphs were constructed by plotting millipolarization units (mP) as a function of protein concentration. Data were analyzed using Prism 4.0 software (Graphpad Software). Compound 3 and the monomeric control compound 2 were evaluated for their ability to displace the fluorescent probe from recombinant protein. Fluorescent probe (5 nM FITC-Smac for XIAP-BIR3 or 1 nM Smac-1F for XIAP-lkBIR2BIR3), and serial dilutions of the two Smac-mimetics (concentration

0.4 nM –4 μM) were added to each well, to a final volume of 125 μl in the assay buffer described above. After mixing on a shaker for 15 min and incubation for 3 h at room temperature, fluorescent polarization was measured with the Ultra plate reader (Tecan).

Microcalorimetric experiments

The binding affinity of compound 2 and compound 3 to the XIAP-BIR2 domain were tested with ITC experiments using VP-ITC technology. Comparable results were obtained for the two compounds (monomeric and dimeric form) with two separate ITC experiments. The measurements were done at 4 °C after 30 consecutive injections of constant volumes (10 μl) of compound 2 (concentrated at 500 μM) or of compound 3 (concentrated at 300 μM) to the protein sample (2 ml, concentrated at 28 μM). The heat measurements were analyzed using the program Origin 7.0 (OriginLab Corporation, One Roundhouse Plaza, Northampton, MA 01060) with a specific package for processing microcalorimetric data (Microcal Origin).

In vitro profiling: cytotoxicity

The HL60 human promyelocytic leukemia cell line was obtained from Interlab Cell Line Collection (ICLC, Genova, Italy). The cell line was cultured at density of 1×10^5 cells/ml in RPMI 1640 medium supplemented with 10% (v/v) fetal bovine serum (FBS) at 37 °C in a 5% (v/v) CO_2 fully humidified atmosphere.

The effect of compound 2 and compound 3 on cell growth was evaluated by means of a colorimetric assay for the quantification of cell proliferation and viability based on the cleavage of the WST-8 tetrazolium salt by mitochondrial dehydrogenases in viable cells (Promokine, Germany). The kits utilize the tetrazolium salts WST-8 that are reduced to water-soluble, orange formazan dyes by dehydrogenases present in viable cells. The absorbance of the formazan dye is proportional to the number of metabolically active cells. Briefly, at time zero and after treatment with Smac-mimetic compounds for 72 h, 10 μl of WST-8 was added to each of the 96-well culture plates containing 1×10^4 cells in 100 μl of complete medium. After incubation at 37 °C for 4 h, the absorbance at 450 nm was measured using a microplate reader 1420 VICTOR multilabel counter (EG&G Wallac, Finland). The data were expressed as mean percentage of three replicates normalized to the untreated control. IC_{50} values were calculated as the concentration of compound inhibiting growth by 50%, relative to control cultures. The results are summarized in Table 1.

cIAP degradation assay

The MDA-MB231 cell line was treated with 5 μM Smac-mimetics or left untreated. After 3 h, cells were harvested and lysed. Proteins were revealed by Western blot with antibodies specific for XIAP (BD Biosciences), cIAP1 (R&DSystems) and βActin (Sigma).

Crystallization

Crystallization trials of XIAP-BIR3 in the presence of various amounts of compound 2 or compound 3 were performed at 20 °C using an Oryx-8 crystallization robot (Douglas Instruments, East Garston, UK) in microbatch plates, that were covered at the end of the experiment with 1.5 ml of paraffin oil and 1.5 ml of Al's oil (50:50 mixture of paraffin oil and silicon oil). Elongated hexagonal prisms of about $100\times30\times30$ μm were obtained only for the XIAP-BIR3/compound 3 complex after two weeks using 20% (w/v) polyethylene glycol monomethyl ether (PEG MME) 2000, 60 mM sodium acetate trihydrate, pH 4.6, 120 mM ammonium sulfate, 400 mM sodium potassium tartrate tetrahydrate. For X-ray data collection, crystals were harvested in a cryoprotectant solution (25% (w/v) PEG MME 2000, 60 mM sodium acetate trihydrate pH 4.6, 120 mM ammonium sulfate, 400 mM sodium potassium tartrate tetrahydrate, 25% (v/v) glycerol) before being flash-cooled in liquid nitrogen. The crystals diffracted to a maximum resolution of 3.0 Å on beamline ID 29 at the European Synchrotron Radiation Facility (ESRF-Grenoble, France).

Structure determination and refinement

The X-ray diffraction data for the XIAP-BIR3/compound 3 complex were indexed (MOSFLM[44]) and scaled, cutting the resolution to 3.0 Å (SCALA[45]) in the trigonal *P*3 space group. A molecular replacement search (PHASER[46]), using the structure of XIAP-BIR3, from the Smac-DIABLO complex (PDB code 1G73[24]), from which the C-terminal α-helix had been deleted (thus retaining amino acids 253–347), was used as search model, locating nine XIAP-BIR3 molecules in space group $P3_1$ (log-likelihood gain = 1081). Rigid body refinement (REFMAC;[47] *R*-factor 44.4%, R_{free} 43.8%) and restrained refinement (*R*-factor 37.6%, R_{free} 41.8%) followed by visual inspection of the map (COOT[48]) showed steric clashes between two of the nine chains, which were therefore omitted from the asymmetric unit model (thus retaining seven model molecules, *R*-factor 36.0%, R_{free} 39.9%). An additional subunit was deleted based on refinement and *B*-factor value considerations (leaving six chains/asymmetric unit, *R*-factor 35.3%, R_{free} 39.0%). Inspection of residual electron density, and the observation that the asymmetric unit at this stage displayed two dimers (interface area 310 $Å^2$) and two isolated chains, helped locating two additional XIAP-BIR3 chains that, together with the isolated ones, yielded two additional dimeric assemblies, for a total of eight asymmetric unit chains (*R*-factor 32.3%, R_{free} 37.0%). Residual map inspection at this stage showed clear electron density close to the IBM groove. Such density allowed us to model compound 3 bound to each molecule in the crystal asymmetric unit. Several refinement cycles (Refmac5 and Buster[49]) and manual rebuilding[48] resulted in the refined model (*R*-factor 23.0%, R_{free} 31.4%) composed of eight BIR3 molecules (amino acids 253±2 through 351±5) and eight compound 3 molecules. The stereochemical quality of the model was checked using the program Procheck.[50]

Thermal shift assays

To monitor protein unfolding, the fluorescent dye Sypro orange was used to monitor the unfolding transition. Using a MiniOpticon Real Time PCR Detection System (Bio-Rad), designed originally for PCR,[51] thermal shift assays were conducted in the presence of the Smac-mimetics. Solutions of 2.4 μl of the purified XIAP-BIR protein constructs (XIAP-BIR2, -BIR3 and -lkBIR2BIR3) were mixed with 3.5 μl of Sypro orange (Sigma) diluted 60-fold, 19 μl of the protein storage buffer and

0.1 μl of 10 mM Smac-mimetics (compounds 2/3). Distilled water was added in place of the inhibitors for the control samples. The final concentrations of protein ranged between 0.5 mg/ml and 5 mg/ml; the sample plates were heated from 25 C to 95 C at a heating rate of 2 degC/min. The fluorescence intensity was measured within the ranges excitation 470–505 nm, emission 540–700 nm.

Analytical gel-filtration experiments

Analytical gel-filtration experiments were done with a Superdex 75 column (GE Healthcare) coupled to an AKTA Purifier system using 20 mM Tris–HCl pH 7.5, 200 mM NaCl, 10 mM DTT. Recombinant XIAP-BIR3 (residues 241–356) was run on the column at a concentration of 1 mg/ml either alone or after incubation for 30 min with an excess of compound 3 (5 mM). The recombinant XIAP-BIR3 and -lkBIR2BIR3 (residues 124–356), each at a concentration of 1 mg/ml, were subsequently run on the column alone or after incubation with 5 mM compound 2 as a control.

Molecular modeling

The AutoDock4 package[38] was used for docking compound 3 to the protein targets, and the Python Molecule Viewer 1.4.5 was used to analyze the data. The XIAP-BIR2[20] (PDB code 1I3O, subunit E) crystal structure was adopted to produce *in silico* models of the XIAP-BIR2/compound 3 complex; the cIAP1-BIR3 crystal structure (PDB code 3D9U, subunit A) was used for the cIAP1-BIR3/compound 3 complex model. A docking grid (32×46×44 points; grid step of 0.375 Å) was centered at Leu207, or Leu307, in XIAP-BIR2 and cIAP1-BIR3, respectively, resulting in a 3416 $Å^3$ box, in which the search was performed. Only one active head of the inhibitor was used to model the protein/compound 3 interactions. During the docking simulation, the protein models were rigidly constrained, whereas 10 rotations around single bonds were allowed for compound 3. The docking procedure consisted of 100 independent genetic algorithm (GA) runs.[38] The three protein/compound 3 docked models displaying the lowest binding free energy were retained for structural analysis.

Model of BIR2-BIR3 in complex with compound 3

The model of XIAP-lkBIR2BIR3 complexed with compound 3 was produced by a simple superposition of two halves of two compound 3 molecules. In particular, rigid translation of subunit D so as to superimpose the head of compound 3 bound to subunit D to the head of compound 3 not bound to subunit B produced a dimeric assembly of subunits B and D bridged by one molecule of inhibitor (Fig. 2b). Finally, the crystal structure of BIR2 (PDB 2VM5) was superimposed on BIR3 subunit D, thereby producing a model of the BIR2-BIR3 assembly in the presence of compound 3. This model (composed of 215 amino acids over 250 of the real assembly) was further used in combination with the SAXS results.

Small-angle X-ray scattering

X-ray scattering data were collected at the beamline SWING of Synchrotron SOLEIL (Gif-sur-Yvette, France). The data were recorded using a CCD-based detector (AVIEX) with a sample-detector distance of 1.84 m, covering the range of momentum transfer $0.012 < q < 0.45$ $Å^{-1}$ ($q = 4\pi \sin\theta\lambda$, where 2θ is the scattering angle and $\lambda = 1.033$ Å the wavelength of the X-rays). XIAP-lkBIR2BIR3 with and without the inhibitor compound 3 was studied in 20 mM Tris–HCl buffer pH 7.5, 200 mM NaCl, 10 mM DTT at protein concentrations between 1 mg/ml and 6 mg/ml. Solutions were circulated continuously during data recording through the 1.8 mm diameter quartz capillary using the automatic sample changer (Agilent) at a flow-rate ensuring an irradiation time of ~1 s. Under these conditions, no radiation damage could be detected in preliminary tests. All measurements were performed at 10 °C. Data were averaged after normalization to the intensity of the transmitted beam before buffer subtraction using the program package PRIMUS.[52] The forward scattering $I(0)$ and the radius of gyration (R_g) were evaluated using the Guinier approximation.[53] The curves of the most dilute, interaction free, and of the most concentrated samples were spliced after scaling to protein concentration to yield a combined, complete scattering pattern. The distance distribution function $p(r)$ corresponds to the distribution of distances between any pair of volume elements within one particle. It was determined using the indirect Fourier transform method as implemented in the program GNOM.[54] The molecular masses of the solutes were evaluated by comparison of the forward scattering with that of a reference 3.9 mg/ml lysozyme solution in 50 mM sodium acetate buffer pH 4.5, 100 mM NaCl.

Low-resolution shapes can be determined using the program Dammin, which describes the protein as a compact assembly of identical dummy atoms.[39] Typically, 10 models are calculated and superimposed using the Damaver suite of routines.[55] They are compared using a measure of similarity called NSD,[56] the smaller the NSD value the higher the similarity. *Ab initio* models were also produced using the program Gasbor, which describes the protein as a chain of N dummy residues, where N is the actual number of protein residues (250 amino acids for XIAP-lkBIR2BIR3).[40] In a way similar to Dammin, 10 models were calculated and compared using NSD values.

Protein Data Bank accession numbers

Atomic coordinates and structure factors have been deposited with the Protein Data Bank with accession number 3G76.[57]

Acknowledgements

This study was supported by grants from the Italian Ministry of University and Research FIRB Project "Biologia Strutturale" (contract RBLA03B3KC_005, to M.B.). We are grateful to Fondazione Associazione Renato Dulbecco for financial support. We thank J. Pérez and G. David (Synchrotron SOLEIL) for help with SAXS measurements. E.M. and M.M. thank the EU/TNA program for travel support to Synchrotron SOLEIL. We are grateful to Elena Casale (Nerviano Medical Sciences, Italy) for invaluable help during the microcalorimetric assays. We thank the European Community Research

Infrastructure Action under the FP6 "Structuring the European Research Area" Programme (through the Integrated Infrastructure Initiative "Integrating Activity on Synchrotron and Free Electron Laser Science") for support.

Supplementary Data

Supplementary data associated with this article can be found, in the online version, at doi:10.1016/j.jmb.2009.04.033

References

1. Steller, H. (1995). Mechanisms and genes of cellular suicide. *Science*, **267**, 1445–1449.
2. Thompson, C. B. (1995). Apoptosis in the pathogenesis and treatment of disease. *Science*, **267**, 1456–1462.
3. Salvesen, G. S. & Abrams, J. M. (2004). Cell death and cancer: an introduction. *Oncogene*, **23**, 2774–2784.
4. Deveraux, Q. L. & Reed, T. C. (1999). IAP family proteins: suppressors of apoptosis. *Gene Dev.* **13**, 239–252.
5. Nicholson, D. W. (2000). From bench to clinic with apoptosis-based therapeutic agents. *Nature*, **407**, 810–816.
6. Okouchi, M., Ekshyyan, O., Maracine, M. & Aw, T. Y. (2007). Neuronal apoptosis in neurodegeneration. *Antioxid. Redox Signal.* **9**, 1059–1096.
7. Ponder, B. A. (2001). Cancer genetics. *Nature*, **411**, 336–341.
8. Liston, P., Fong, W. G. & Korneluk, R. G. (2003). The inhibitors of apoptosis: there is more to life than Bcl2. *Oncogene*, **22**, 8568–8580.
9. Salvesen, G. S. & Duckett, C. S. (2002). IAP proteins: blocking the road to death's door. *Nature Rev. Mol. Cell Biol.* **3**, 401–4010.
10. Vaux, D. L. & Silke, J. (2005). IAPs, RINGs and ubiquitylation. *Nat. Rev. Mol. Cell Biol.* **6**, 287–297.
11. Hofmann, K., Bucher, P. & Tschopp, J. (1997). The CARD domain: a new apoptotic signalling motif. *Trends Biochem. Sci.* **22**, 155–156.
12. Shu, H. B., Takeuchi, M. & Goeddel, D. V. (1996). The tumor necrosis factor receptor 2 signal transducers TRAF2 and c-IAP1 are components of the tumor necrosis factor receptor 1 signaling complex. *Proc. Natl Acad. Sci. USA*, **93**, 13973–13978.
13. Wang, C. Y., Mayo, M. W., Korneluk, R. G., Goeddel, D. V. & Baldwin, A. S., Jr (1998). NF-kappaB antiapoptosis: induction of TRAF1 and TRAF2 and c-IAP1 and c-IAP2 to suppress caspase-8 activation. *Science*, **281**, 1680–1683.
14. Rothe, M., Pan, M. G., Henzel, W. J., Ayres, T. M. & Goeddel, D. V. (1995). The TNFR2-TRAF signaling complex contains two novel proteins related to baculoviral inhibitor of apoptosis proteins. *Cell*, **83**, 1243–1252.
15. Samuel, T., Welsh, K., Lober, T., Togo, S. H., Zapata, J. M. & Reed, J. C. (2006). Distinct BIR domains of cIAP1 mediate binding to and ubiquitination of tumor necrosis factor receptor-associated factor 2 and second mitochondrial activator of caspases. *J. Biol. Chem.* **281**, 1080–1090.
16. Varfolomeev, E., Blankenship, J. W., Wayson, S. M., Fedorova, A. V., Kayagaki, N., Garg, P. *et al.* (2007). IAP antagonists induce autoubiquitination of c-IAPs, NF-kappaB activation, and TNFalpha-dependent apoptosis. *Cell*, **131**, 669–681.
17. Tamm, I., Kornblau, S. M., Segall, H., Krajewski, S., Welsh, K., Kitada, S. *et al.* (2000). Expression and prognostic significance of IAP-family genes in human cancers and myeloid leukemias. *Clin. Cancer Res.* **6**, 1796–1803.
18. Vischioni, B., van der Valk, P., Span, S. W., Kruyt, F. A., Rodriguez, J. A. & Giaccone, G. (2006). Expression and localization of inhibitor of apoptosis proteins in normal human tissues. *Hum. Pathol.* **37**, 78–86.
19. Shiozaki, E. N., Chai, J., Rigotti, D. J., Riedl, S. J., Li, P., Srinivasula, S. M. *et al.* (2003). Mechanism of XIAP-mediated inhibition of caspase-9. *Mol. Cell*, **11**, 519–527.
20. Riedl, S. J., Renatus, M., Schwarzenbacher, R., Zhou, Q., Sun, C., Fesik, S. W. *et al.* (2001). Structural basis for the inhibition of caspase-3 by XIAP. *Cell*, **104**, 791–800.
21. Huang, Y., Park, Y. C., Rich, R. L., Segal, D., Myszka, D. G. & Wu, H. (2001). Structural basis of caspase inhibition by XIAP: differential roles of the linker versus the BIR domain. *Cell*, **104**, 781–790.
22. Du, C., Fang, M., Li, Y., Li, L. & Wang, X. (2000). Smac, a mitochondrial protein that promotes cytochrome c-dependent caspase activation by eliminating IAP inhibition. *Cell*, **102**, 33–42.
23. Verhagen, A. M., Ekert, P. G., Pakusch, M., Silke, J., Connolly, L. M., Reid, G. E. *et al.* (2000). Identification of DIABLO, a mammalian protein that promotes apoptosis by binding to and antagonizing IAP proteins. *Cell*, **102**, 43–53.
24. Wu, G., Chai, J., Suber, T. L., Wu, J. W., Du, C., Wang, X. & Shi, Y. (2000). Structural basis of IAP recognition by Smac/DIABLO. *Nature*, **408**, 1008–1012.
25. Sun, H., Nikolovska-Coleska, Z., Yang, C. Y., Xu, L., Liu, M., Tomita, Y. *et al.* (2004). Structure-based design of potent, conformationally constrained Smac mimetics. *J. Am. Chem. Soc.* **126**, 16686–16687.
26. Wist, A. D., Gu, L., Riedl, S. J., Shi, Y. & McLendon, G. L. (2007). Structure-activity based study of the Smac-binding pocket within the BIR3 domain of XIAP. *Bioorg. Med. Chem.* **15**, 2935–2943.
27. Li, L., Thomas, R. M., Suzuki, H., De Brabander, J. K., Wang, X. & Harran, P. G. (2004). A small molecule Smac mimic potentiates TRAIL- and TNFalpha-mediated cell death. *Science*, **305**, 1471–1474.
28. Sun, H., Nikolovska-Coleska, Z., Lu, J., Meagher, J. L., Yang, C. Y., Qiu, S. *et al.* (2007). Design, synthesis, and characterization of a potent, nonpeptide, cell-permeable, bivalent Smac mimetic that concurrently targets both the BIR2 and BIR3 domains in XIAP. *J. Am. Chem. Soc.* **129**, 15279–15294.
29. Petersen, S. L., Wang, L., Yalcin-Chin, A., Li, L., Peyton, M., Minna, J. *et al.* (2007). Autocrine TNFalpha signaling renders human cancer cells susceptible to Smac-mimetic-induced apoptosis. *Cancer Cell*, **12**, 445–456.
30. Cossu, F., Mastrangelo, E., Milani, M., Sorrentino, G., Lecis, D., Delia, D. *et al.* (2009). Designing Smac-mimetics as antagonists of XIAP, cIAP1, and cIAP2. *Biochem. Biophys. Res. Commun.* **378**, 162–167.
31. Mastrangelo, E., Cossu, F., Milani, M., Sorrentino, G., Lecis, D., Delia, D. *et al.* (2008). Targeting the X-linked inhibitor of apoptosis protein through 4-substituted azabicyclo[5.3.0]alkane smac mimetics. Structure, activity, and recognition principles. *J. Mol. Biol.* **384**, 673–689.
32. Sun, H., Stuckey, J. A., Nikolovska-Coleska, Z., Qin, D., Meagher, J. L., Qiu, S. *et al.* (2008). Structure-based

design, synthesis, evaluation, and crystallographic studies of conformationally constrained Smac mimetics as inhibitors of the X-linked inhibitor of apoptosis protein (XIAP). *J. Med. Chem.* **51**, 7169–7180.
33. Nikolovska-Coleska, Z., Meagher, J. L., Jiang, S., Yang, C. Y., Qiu, S., Roller, P. P. *et al.* (2008). Interaction of a cyclic, bivalent smac mimetic with the x-linked inhibitor of apoptosis protein. *Biochemistry*, **47**, 9811–9824.
34. Nikolovska-Coleska, Z., Meagher, J. L., Jiang, S., Kawamoto, S. A., Gao, W., Yi, H. *et al.* (2008). Design and characterization of bivalent Smac-based peptides as antagonists of XIAP and development and validation of a fluorescence polarization assay for XIAP containing both BIR2 and BIR3 domains. *Anal. Biochem.* **374**, 87–98.
35. Nikolovska-Coleska, Z., Wang, R., Fang, X., Pan, H., Tomita, Y., Li, P. *et al.* (2004). Development and optimization of a binding assay for the XIAP BIR3 domain using fluorescence polarization. *Anal. Biochem.* **332**, 261–273.
36. Cantor, C. R. & Schimmel, P. R. (1980). The behavior of biological macromolecules. In *Biophysical Chemistry*, part III, pp. 850-852, Freeman, W. H. & Co, San Francisco, CA.
37. Pantoliano, M. W., Petrella, E. C., Kwasnoski, J. D., Lobanov, V. S., Myslik, J., Graf, E. *et al.* (2001). High-density miniaturized thermal shift assays as a general strategy for drug discovery. *J. Biomol. Screen.* **6**, 429–440.
38. Morris, G. M., Goodsell, D. S., Halliday, R. S., Huey, R., Hart, W. E., Belew, R. K. & Olson, A. J. (1998). Automated docking using a Lamarckian genetic algorithm and an empirical binding free energy function. *J. Comput. Chem.* **19**, 1639–1662.
39. Svergun, D. I. (1999). Restoring low resolution structure of biological macromolecules from solution scattering using simulated annealing. *Biophys. J.* **76**, 2879–2886.
40. Svergun, D. I., Petoukhov, M. V. & Koch, M. H. (2001). Determination of domain structure proteins from X-ray solution scattering. *Biophys. J.* **80**, 2946–2953.
41. Vince, J. E., Wong, W. W., Khan, N., Feltham, R., Chau, D., Ahmed, A. U. *et al.* (2007). IAP antagonists target cIAP1 to induce TNFalpha-dependent apoptosis. *Cell*, **131**, 682–693.
42. Kulathila, R., Vash, B., Sage, D., Cornell-Kennon, S., Wright, K., Koehn, J. *et al.* (2009). The crystal structure of the BIR3 domain from cIAP1 in complex with the N-terminal peptide of SMAC and Caspase-9. *Acta Cryst. D*, **65**, 58–66.
43. Wang, L., Du, F. & Wang, X. (2008). TNF-alpha induces two distinct caspase-8 activation pathways. *Cell*, **133**, 693–703.
44. Steller, I, Bolotovsky, R & MG, R. (1997). An algorithm for automatic indexing of oscillation images using Fourier analysis. *J. Appl. Crystallogr.* **30**, 1036–1040.
45. Collaborative Computational Project, Number 4. (1994). The CCP4 suite: programs for protein crystallography. *Acta Crystallog. D*, **50**, 760–763.
46. McCoy, A. J., Grosse-Kunstleve, R. W., Adams, P. D., Winn, M. D., Storoni, L. C. & Read, R. J. (2007). Phaser crystallographic software. *J. Appl. Crystallogr.* **40**, 658–674.
47. Winn, M. D., Isupov, M. N. & Murshudov, G. N. (2001). Use of TLS parameters to model anisotropic displacements in macromolecular refinement. *Acta Crystallogr. D*, **57**, 122–133.
48. Emsley, P. & Cowtan, K. (2004). Coot: model-building tools for molecular graphics. *Acta Crystallogr. D*, **60**, 2126–2132.
49. Roversi, P., Blanc, E., Vonrhein, C., Evans, G. & Bricogne, G. (2000). Modelling prior distributions of atoms for Macromolecular Refinement and Completion. *Acta Crystallogr. D*, **56**, 1313–1323.
50. Laskowski, R. A., Rullmannn, J. A., MacArthur, M. W., Kaptein, R. & Thornton, J. M. (1996). AQUA and PROCHECK-NMR: programs for checking the quality of protein structures solved by NMR. *J. Biomol. NMR*, **8**, 477–486.
51. Lo, M. C., Aulabaugh, A., Jin, G., Cowling, R., Bard, J., Malamas, M. & Ellestad, G. (2004). Evaluation of fluorescence-based thermal shift assays for hit identification in drug discovery. *Anal. Biochem.* **332**, 153–159.
52. Konarev, P. V., Volkov, V. V., Sokolova, A. V., Koch, M. H. J. & Svergun, D. I. (2003). PRIMUS: a Windows PC-based system for small-angle scattering data analysis. *J. Appl. Crystallogr.* **36**, 1277–1282.
53. Guinier, A. (1939). Diffraction of X-rays of very small angles – application to the study of ultramicroscopic phenomenon. *Ann. Phys.* **12**, 161–237.
54. Svergun, D. I. (1992). Determination of the regularization parameter in indirect-transform methods using perceptual criteria. *J. Appl. Crystallogr.* **25**, 495–503.
55. Volkov, V. V. & Svergun, D. I. (2003). Uniqueness of ab initio shape determination in small-angle scattering. *J. Appl. Crystallogr.* **36**, 860–864.
56. Kozin, M. B. & Svergun, D. I. (2001). Automated matching of high- and low- resolution structural models. *J. Appl. Crystallogr.* **34**, 33–41.
57. Berman, H. M., Westbrook, J., Feng, Z., Gilliland, G., Bhat, T. N., Weissig, H. *et al.* (2000). The Protein Data Bank. *Nucleic Acids Res.* **28**, 235–242.
58. Potterton, E., McNicholas, S., Krissinel, E., Cowtan, K. & Noble, M. (2002). The CCP4 molecular-graphics project. *Acta Crystallogr. D*, **58**, 1955–1957.